

Light-Induced Mirror Symmetry Breaking and Charge Transport

Naoya Arakawa^{1*}, Kenji Yonemitsu^{1,2}

¹The Institute of Science and Engineering, Chuo University, Bunkyo, Tokyo, 112-8551, Japan

²Department of Physics, Chuo University, Bunkyo, Tokyo 112-8551, Japan

We propose that light can break mirror symmetries and combining symmetries with a uniform time translation, and their breaking is characterized by an off-diagonal charge conductivity. Taking periodically driven graphene as an example, we show that mirror symmetries about the xz and yz planes and the combining symmetries, the symmetries of combinations of the mirror operations about these planes and a uniform time translation, can be broken by linearly or circularly polarized light. We also show that this symmetry breaking induces the time-averaged off-diagonal symmetric or antisymmetric charge conductivity in a nonequilibrium steady state with linearly or circularly, respectively, polarized light. Our results are experimentally testable in pump-probe measurements. This work will pave the way for controlling mirror symmetries via light and utilizing the light-induced mirror symmetry breaking.

1. Introduction

Light can break symmetries in time and space. For example, circularly polarized light (CPL) can break the time-reversal symmetry.¹⁻³⁾ If CPL is applied to a non-magnetic material, it can induce the magnetization;⁴⁾ the direction of this light-induced magnetization can be reversed by changing the helicity of CPL.⁵⁾ CPL can also induce the anomalous Hall effect (AHE),^{6,7)} in which a charge current perpendicular to an applied electric field is generated;⁸⁻¹⁰⁾ the magnitude and direction of this current can be changed by varying the amplitude and helicity of CPL.^{6,7,11,12)} Then, bicircularly polarized light,^{13,14)} which consists of a linear combination of left-handed and right-handed CPL, can break not only the time-reversal, but also the inversion symmetry.¹⁵⁾ In fact, it can be used to realize noncentrosymmetric magnetic topological phases¹⁵⁾ and generate electric polarization.¹⁶⁾ Since the application of light enables us to engineer electronic, magnetic, or transport properties without changing materials, it is crucial to understand which symmetry is broken by light and how its symmetry breaking affects the properties.

In this paper, we show the mirror symmetry breaking by CPL or by linearly polarized light (LPL), which results in an off-diagonal antisymmetric or symmetric, respectively, charge conductivity (i.e., $\sigma_{xy}^C = -\sigma_{yx}^C$ or $\sigma_{xy}^C = \sigma_{yx}^C$, respectively). This is demonstrated for periodically driven graphene. The difference between the cases with CPL and LPL comes from the difference in the time-reversal symmetry. The main results are summarized in Table I. Our results suggest that a combination of time-reversal symmetry breaking and mirror symmetry breaking is the origin of the light-induced AHE, and that the off-diagonal symmetric charge conductivity could be used to detect whether mirror symmetries are broken or preserved in the presence of the time-reversal symmetry.

Table I. Properties of systems driven by CPL or LPL. The difference among LPL1, LPL2, and LPL3 is about the polarization: $A_x \neq 0$ and $A_y \neq 0$ in LPL1; $A_x \neq 0$ and $A_y = 0$ in LPL2; and $A_x = 0$ and $A_y \neq 0$ in LPL3. T_{rev} represents the time-reversal symmetry, σ_m or σ'_m represents the mirror symmetry about the xz or yz plane, respectively, and C_3 represents the C_3 rotational symmetry around the z axis. $\sigma_m T_t$, $\sigma'_m T_t$, or $C_3 T_t$ represents the symmetry of a combination of the mirror operation about the xz or yz plane or the C_3 rotation operation and a uniform time translation T_t . σ_{yx}^C represents an off-diagonal charge conductivity. $\sigma_m T_t$ or $\sigma'_m T_t$ is preserved with LPL3 or LPL2, respectively, if $T_t : t \rightarrow t - \frac{\pi}{\Omega}$. $C_3 T_t$ is preserved with CPL if $T_t : t \rightarrow t + \frac{2\pi}{3\Omega}$.

	CPL	LPL1	LPL2	LPL3
T_{rev}	Broken	Preserved	Preserved	Preserved
σ_m	Broken	Broken	Preserved	Broken
$\sigma_m T_t$	Broken	Broken	Preserved	Preserved
σ'_m	Broken	Broken	Broken	Preserved
$\sigma'_m T_t$	Broken	Broken	Preserved	Preserved
C_3	Broken	Broken	Broken	Broken
$C_3 T_t$	Preserved	Broken	Broken	Broken
σ_{yx}^C	Antisymmetric	Symmetric	Vanishing	Vanishing

2. Model

Our periodically driven electron system is described by the Hamiltonian,

$$H = H_s(t) + H_b + H_{\text{sb}}. \quad (1)$$

Here $H_s(t)$ is the Hamiltonian of the system driven by a light field $\mathbf{A}(t)$, the effect of which is treated as the Peierls phase factors:

$$H_s(t) = \sum_{\mathbf{k}} \sum_{a,b=A,B} \sum_{\sigma=\uparrow,\downarrow} \epsilon_{ab}(\mathbf{k}, t) c_{\mathbf{k}a\sigma}^\dagger c_{\mathbf{k}b\sigma}, \quad (2)$$

*E-mail address: arakawa@phys.chuo-u.ac.jp

where $\epsilon_{AB}(\mathbf{k}, t) = \epsilon_{BA}(\mathbf{k}, t)^* = t_{\text{NN}} \sum_{l=0}^2 e^{-i[\mathbf{k} + e\mathbf{A}(t)] \cdot \mathbf{R}_l}$, $\epsilon_{aa}(\mathbf{k}, t) = 0$, $\mathbf{R}_0 = {}^t(0, 1)$, $\mathbf{R}_1 = {}^t(-\frac{\sqrt{3}}{2}, -\frac{1}{2})$, $\mathbf{R}_2 = {}^t(\frac{\sqrt{3}}{2}, -\frac{1}{2})$, t_{NN} is the hopping integral between nearest neighbor sites on a honeycomb lattice¹⁷⁾ without $\mathbf{A}(t)$, and $c_{\mathbf{k}a\sigma}^\dagger$ and $c_{\mathbf{k}a\sigma}$ are the creation and annihilation operators of an electron for momentum \mathbf{k} , sublattice a , and spin σ . Hereafter, we set $\hbar = c = k_{\text{B}} = a_{\text{NN}} = 1$, where a_{NN} is the length between nearest neighbor sites. Then, H_{b} is the Hamiltonian of the Buttiker-type heat bath,^{18,19)} which is in equilibrium at temperature T : $H_{\text{b}} = \sum_i \sum_p (\epsilon_p - \mu_{\text{b}}) b_{i p}^\dagger b_{i p}$, where $b_{i p}$ and $b_{i p}^\dagger$ are the annihilation and creation operators of a bath's fermion at site i for mode p , and ϵ_p and μ_{b} are the energy and chemical potential of a bath's fermion; μ_{b} is determined from the condition that there is no current between the system and bath. In addition, H_{sb} is the system-bath coupling Hamiltonian:^{11,12,20)} $H_{\text{sb}} = \sum_i \sum_p \sum_{a=A,B} \sum_{\sigma=\uparrow,\downarrow} V_{pa\sigma} (c_{i a\sigma}^\dagger b_{i p} + b_{i p}^\dagger c_{i a\sigma})$, where $V_{pa\sigma}$ is the system-bath coupling constant.

We have considered H_{b} and H_{sb} , as well as $H_{\text{s}}(t)$, because the damping due to the system-bath coupling makes the system a nonequilibrium steady state.^{11,12,20)} Such a relaxation mechanism is necessary for periodically driven systems, in which the heating due to the driving field exists.^{21,22)}

3. Light-induced mirror symmetry breaking

First, we analyze the polarization dependence of the light-induced mirror symmetry breaking. For our periodically driven electron system, whether a mirror symmetry is preserved or broken is determined by the symmetry of the kinetic energy, which is characterized by

$$\epsilon_{AB}(\mathbf{k}, t) = t_{AB}^Z(t) e^{-ik_y} + t_{AB}^X(t) e^{i\frac{\sqrt{3}}{2}k_x} e^{i\frac{k_y}{2}} + t_{AB}^Y(t) e^{-i\frac{\sqrt{3}}{2}k_x} e^{i\frac{k_y}{2}}, \quad (3)$$

$$\epsilon_{BA}(\mathbf{k}, t) = t_{BA}^Z(t) e^{ik_y} + t_{BA}^X(t) e^{-i\frac{\sqrt{3}}{2}k_x} e^{-i\frac{k_y}{2}} + t_{BA}^Y(t) e^{i\frac{\sqrt{3}}{2}k_x} e^{-i\frac{k_y}{2}}, \quad (4)$$

where $t_{AB}^Z(t) = t_{BA}^Z(t)^*$, $t_{AB}^X(t) = t_{BA}^X(t)^*$, and $t_{AB}^Y(t) = t_{BA}^Y(t)^*$. Here Z , X , and Y represent the three bonds between nearest neighbor sites (see Fig. 1). If the hopping integrals satisfy

$$t_{AB}^Z(t) = t_{BA}^Z(t), t_{AB}^Y(t) = t_{BA}^Y(t), t_{AB}^X(t) = t_{BA}^X(t), \quad (5)$$

the mirror symmetry about the xz plane [Fig. 1(a)] is preserved; otherwise, it is broken.

We begin with the system driven by LPL. The field of LPL is described by

$$\mathbf{A}_{\text{pump}}(t) = {}^t(A_0 \alpha_x \cos \Omega t \ A_0 \alpha_y \cos \Omega t), \quad (6)$$

where $\Omega = 2\pi/T_{\text{p}}$ is the light frequency, and T_{p} is the period of $\mathbf{A}_{\text{pump}}(t)$. In this case, $t_{AB}^Z(t) = t_{\text{NN}} e^{-iu\alpha_y \cos \Omega t}$, $t_{AB}^X(t) = t_{\text{NN}} e^{iu\alpha_x \frac{\sqrt{3}}{2} \cos \Omega t} e^{iu\alpha_y \frac{1}{2} \cos \Omega t}$, and $t_{AB}^Y(t) = t_{\text{NN}} e^{-iu\alpha_x \frac{\sqrt{3}}{2} \cos \Omega t} e^{iu\alpha_y \frac{1}{2} \cos \Omega t}$, where $u = eA_0$. For the LPL with $\alpha_x \neq 0$, $\alpha_y = 0$, these hopping integrals satisfy Eq. (5), which means that the mirror symmetry about the xz plane is preserved. Meanwhile, for the LPL with

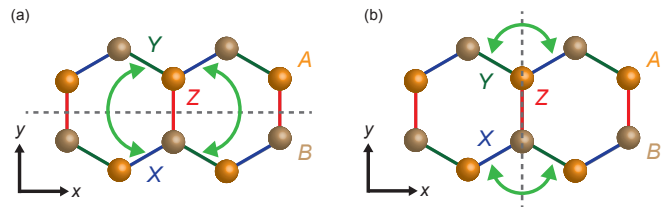


Fig. 1. (Color online) The honeycomb lattice and (a) the xz or (b) the yz mirror plane. The dashed lines denote the mirror planes. The green arrows represent the bonds which are connected by the mirror symmetry. A or B represents sublattice A or B , respectively. The red, blue, and dark green bonds represent Z , X , and Y bonds, respectively. The x and y axes are also drawn.

$\alpha_x = 0$, $\alpha_y \neq 0$ or with $\alpha_x \neq 0$, $\alpha_y \neq 0$, this mirror symmetry is broken.

We turn to the case with CPL. The field of CPL is given by

$$\mathbf{A}_{\text{pump}}(t) = {}^t(A_0 \cos \Omega t \ A_0 \sin \Omega t). \quad (7)$$

In a similar way, we can show that the mirror symmetry about the xz plane is broken.

We make five remarks. First, we can similarly show that the mirror symmetry about the yz plane [Fig. 1(b)] is broken by LPL with $\alpha_x \neq 0$, $\alpha_y = 0$, by that with $\alpha_x \neq 0$, $\alpha_y \neq 0$, and by CPL, whereas it is preserved by LPL with $\alpha_x = 0$, $\alpha_y \neq 0$. Second, the same polarization dependence holds for the Floquet Hamiltonian (see Appendix A). Third, the similar arguments can be used to discuss whether a mirror symmetry is broken or not in the other periodically driven electron systems. Fourth, a mirror symmetry of a periodically driven electron system does not necessarily match that of the trajectory of $\mathbf{A}_{\text{pump}}(t)$. For example, CPL breaks the mirror symmetry about the xz plane, whereas the trajectory of its $\mathbf{A}_{\text{pump}}(t)$ has the mirror symmetry in the A_x - A_y plane [see Fig. 2(a)]. Fifth, our mirror symmetry, the symmetry about a mirror operation in crystals, is essentially different from a symmetry discussed in Ref.,²³⁾ the symmetry about the energy spectrum as a function of magnetic flux. Namely, the light-induced symmetry breaking discussed in Ref.²³⁾ is not about crystal's mirror symmetry. To the best of our knowledge, our paper is the first work demonstrating the light-induced breaking of crystal's mirror symmetry.

The above arguments show that the mirror symmetries about the xz and yz planes are broken with CPL or LPL1 (i.e., LPL with finite α_x and α_y). To study a time-averaged quantity in a nonequilibrium steady state, we need to discuss not only the mirror symmetries, but also its combining symmetries, the symmetries of combinations of the mirror operations about the xz and yz planes and a uniform time translation, because that quantity is not affected by such a translation. (Note that such a combining symmetry is sometimes called a space-time or dynamical symmetry.) In general, there is a case that a spatial symmetry is broken, but its combining symmetry is preserved; in such a case, a time-averaged quantity in a nonequilibrium steady state behaves as if the spatial symmetry were preserved. As we show in Appendix

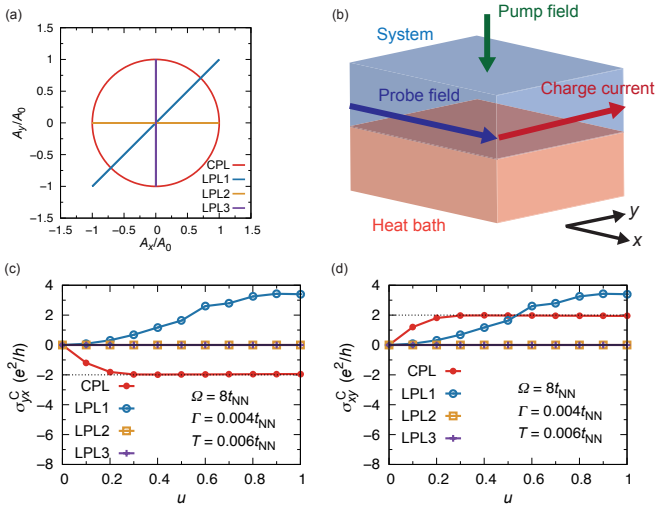


Fig. 2. (Color online) (a) The trajectories of $\mathbf{A}_{\text{pump}}(t)$ for CPL, LPL1, LPL2, and LPL3. (b) The setup for the pump-probe measurements of σ_{yx}^C in our periodically driven system. For the setup of σ_{xy}^C , the directions of the probe field and charge current are interchanged. The arrow of the pump light indicates the direction of travel, and that of the probe light indicates the direction of the component of the corresponding electric field. (c), (d) σ_{yx}^C and σ_{xy}^C as functions of $u = eA_0$ for graphene driven by CPL, LPL1, LPL2, and LPL3. The horizontal dashed lines in (c) and (d) correspond to $-2e^2h^{-1}$ and $2e^2h^{-1}$, respectively.

B, the combining symmetries for the mirror operations are also broken with CPL or LPL1. This contrasts with the combining symmetry for the C_3 rotation in graphene driven by CPL (see Appendix B): the C_3 rotational symmetry is broken, but the symmetry of a combination of the C_3 rotation and the uniform time translation $T_t : t \rightarrow t + \frac{2\pi}{3\Omega}$ is preserved.¹¹⁾ This combining symmetry may be called a time-screw symmetry. In appendix B, we also show that the combining symmetry for the mirror operation about the yz or xz plane is preserved with LPL2 (i.e., LPL with $\alpha_x \neq 0, \alpha_y = 0$) or LPL3 (i.e., LPL with $\alpha_x = 0, \alpha_y \neq 0$), respectively, if $T_t : t \rightarrow t - \frac{\pi}{\Omega}$. This combining symmetry may be called a time-glide symmetry. We do not necessarily call the combining symmetry for a mirror operation a time-glide one because an analogy with an axial glide symmetry suggests that a time-glide symmetry consists of a mirror operation and the uniform time translation with $T_p/2$. Then, the C_3 rotational symmetry and its combining symmetry are both broken with LPL (see Appendix B). These results are summarized in Table I.

4. Charge transport induced by mirror symmetry breaking

Next, we study the effects of the light-induced mirror symmetry breaking on transport properties. To do this, we use the Floquet linear-response theory^{11,12,24)} for pump-probe measurements [Fig. 2(b)]. In this theory, we set $\mathbf{A}(t) = \mathbf{A}_{\text{pump}}(t) + \mathbf{A}_{\text{prob}}(t)$ and treat the effects of $\mathbf{A}_{\text{pump}}(t)$ in the Floquet theory^{25,26)} and those of $\mathbf{A}_{\text{prob}}(t)$ in the linear-response theory.²⁷⁾ The $\mathbf{A}_{\text{pump}}(t)$ for LPL or CPL is given by Eq. (6) or (7), respectively. Note that $\mathbf{A}_{\text{pump}}(t)$ is used to periodically drive the

system, whereas $\mathbf{A}_{\text{prob}}(t)$ is used to analyze its properties.²⁸⁾ In this theory, we use the Floquet Hamiltonian for $H_s(t)$, which is distinct from the Hamiltonian obtained in a high-frequency expansion. Using the Floquet linear-response theory, we obtain a time-averaged charge conductivity $\sigma_{\mu\nu}^C$ in the nonequilibrium steady state^{11,12)} (see Appendix C),

$$\sigma_{\mu\nu}^C = \frac{e^2}{V} \sum_{\mathbf{k}} \sum_{a,b,c,d=A,B} \sum_{\sigma,\sigma'=\uparrow,\downarrow} \int_{-\Omega/2}^{\Omega/2} \frac{d\omega'}{2\pi} \times \text{tr} \left[v_{ab}^{\mu}(\mathbf{k}) \frac{\partial G_{b\sigma c\sigma'}^R(\mathbf{k}, \omega')}{\partial \omega'} v_{cd}^{\nu}(\mathbf{k}) G_{d\sigma' a\sigma}^<(\mathbf{k}, \omega') - v_{ab}^{\mu}(\mathbf{k}) G_{b\sigma c\sigma'}^<(\mathbf{k}, \omega') v_{cd}^{\nu}(\mathbf{k}) \frac{\partial G_{d\sigma' a\sigma}^A(\mathbf{k}, \omega')}{\partial \omega'} \right], \quad (8)$$

where the trace is taken over the Floquet states [i.e., $\text{tr}(ABCD) = \sum_{m,l,n,q=-\infty}^{\infty} A_{ml} B_{ln} C_{nq} D_{qm}$ with Floquet indices m, l, n , and q], $V = \frac{N}{2} \frac{3\sqrt{3}}{2}$, N is the number of sites, $[v_{ab}^{\nu}(\mathbf{k})]_{mn}$ is the group velocity in the Floquet representation, and $[G_{a\sigma b\sigma'}^R(\mathbf{k}, \omega')]_{mn}$, $[G_{a\sigma b\sigma'}^A(\mathbf{k}, \omega')]_{mn}$, and $[G_{a\sigma b\sigma'}^<(\mathbf{k}, \omega')]_{mn}$ are the retarded, advanced, and lesser Green's functions, respectively, in the Floquet representation. (For more details, see Appendix C.) These Green's functions are determined from Dyson's equation with the damping Γ due to the second-order perturbation of H_{sb} (see Appendix D). Note that $\sigma_{\mu\nu}^C$ is equivalent to the anomalous Hall conductivity if and only if it is anti-symmetric.

Using Eq. (8), we numerically evaluate σ_{yx}^C and σ_{xy}^C for graphene driven by CPL, LPL1, LPL2, and LPL3. (For details of the numerical calculations, see Appendix E.) The directions of the probe field and the observed charge current are fixed: for σ_{yx}^C (or σ_{xy}^C), the charge current along the y (or x) axis is generated with the probe field applied along the x (or y) axis. CPL is described by Eq. (7), and LPL1, LPL2, or LPL3 is described by Eq. (6) with $\alpha_x = \alpha_y = 1$, with $\alpha_x = 1$ and $\alpha_y = 0$, or with $\alpha_x = 0$ and $\alpha_y = 1$, respectively [Fig. 2(a)]; as described above, the mirror symmetry about the xz or yz plane is preserved only for LPL2 or LPL3, respectively. We set $\Omega = 8t_{\text{NN}}$ and $t_{\text{NN}} = 1$; our light is off-resonant, i.e., $\Omega > W$, where $W (= 6t_{\text{NN}})$ is the bandwidth without light. (We have summarized the main results in Table I.) Except for the results of the damping or temperature dependence of σ_{yx}^C with LPL1, we set $\Gamma = 0.004t_{\text{NN}}$ and $T = 0.006t_{\text{NN}}$. When discussing the damping dependence, we set $T = 0.006t_{\text{NN}}$ and compare the results obtained at $\Gamma = 0.004t_{\text{NN}}, 0.002t_{\text{NN}}$, and $0.006t_{\text{NN}}$; when discussing the temperature dependence, we set $\Gamma = 0.004t_{\text{NN}}$ and compare the results obtained at $T = 0.006t_{\text{NN}}, 0.004t_{\text{NN}}$, and $0.008t_{\text{NN}}$.

Figure 2(c) shows the u dependences of σ_{yx}^C in graphene driven by CPL, LPL1, LPL2, and LPL3. σ_{yx}^C for $u \neq 0$ is finite for CPL and LPL1, whereas it vanishes for LPL2 and LPL3. The similar results are obtained also for σ_{xy}^C [Fig. 2(d)]. These results are consistent with the properties of the mirror symmetries about the xz and yz planes and their combining symmetries (see Table I). Therefore, the mirror symmetries and their combining symmetries play a vital role in discussing the off-diagonal

charge conductivities. Note that since $u = eA_0 = eE_0/\Omega$ is dimensionless, the u dependence of σ_{yx}^C at fixed Ω gives its dependence on E_0 , the amplitude of the light field.

One of the main differences between the cases of CPL and LPL1 is the relation between σ_{yx}^C and σ_{xy}^C . Figure 2(d) shows the u dependences of σ_{xy}^C in graphene driven by CPL, LPL1, LPL2, and LPL3. Comparing this figure with Fig. 2(c), we see that $\sigma_{xy}^C = -\sigma_{yx}^C$ for CPL, whereas $\sigma_{xy}^C = \sigma_{yx}^C$ for LPL1. They are the Onsager reciprocal relations,^{29,30} and their difference comes from the difference in the time-reversal symmetry. We should note that $\sigma_{xy}^C = \sigma_{yx}^C$ for LPL1 does not contradict the properties of the C_3 rotational symmetry (see Appendix B). Since the anomalous Hall conductivity is off-diagonal and antisymmetric, our results indicate that the light-induced AHE comes from a combination of mirror symmetry breaking and time-reversal symmetry breaking. This is consistent with the AHE in nondriven systems.^{31,32} Our results also suggest that the off-diagonal symmetric charge conductivity can be regarded as an indicator for mirror symmetry breaking in the presence of the time-reversal symmetry. This might be used to detect helical higher-order topological insulators,³³ which are protected by the mirror symmetry and time-reversal symmetry, because that conductivity vanishes with the mirror symmetry or its combining symmetry, as shown above.

Another difference is about the quantization of σ_{yx}^C . σ_{yx}^C is quantized only with CPL. This quantization can be understood using a high-frequency expansion,^{34,35} as shown in previous studies:^{11,36} the term proportional to Ω^{-1} gives a pure-imaginary hopping integral between next-nearest neighbors on the honeycomb lattice, which is similar to the term vital for the quantum Hall effect.³⁷ Similarly, we can understand the non-quantized σ_{yx}^C with LPL: the Ω^{-1} term becomes zero. This is consistent with the property that LPL does not break the time-reversal symmetry. Note that except the above interpretations, we do not use the high-frequency expansion.

The other difference is about the Γ dependence of σ_{yx}^C . Figure 3(a) shows the Γ dependence of σ_{yx}^C for graphene driven by LPL1. σ_{yx}^C is roughly proportional to Γ^{-1} . This contrasts the Γ dependence of the off-diagonal charge conductivity for graphene driven by CPL because it is almost independent of Γ [e.g., compare the red curve in Fig. 2(d) of this paper and the brown one in Fig. 10 of Ref.¹¹]. Note that σ_{yx}^C with LPL1, as well as that with CPL, is little dependent on the bath temperature T [Fig. 3(b)]. This is because the bath temperature may play a similar role to the temperature appearing in the distribution function. We should note that Γ is independent of temperature in our theory.

The sign of the off-diagonal symmetric charge conductivity can be reversed by replacing LPL1 by the LPL for $\alpha_x = -\alpha_y = 1$ or $-\alpha_x = \alpha_y = 1$, a counterpart connected by the mirror operation about the xz or yz plane, respectively. Furthermore, it remains unchanged by replacing LPL1 by the LPL for $\alpha_x = \alpha_y = -1$. The similar properties hold for arbitrary θ when $\alpha_x = \cos\theta$ and $\alpha_y = \sin\theta$. These three additional results are shown in Appendix F. They also suggest the vital role of the

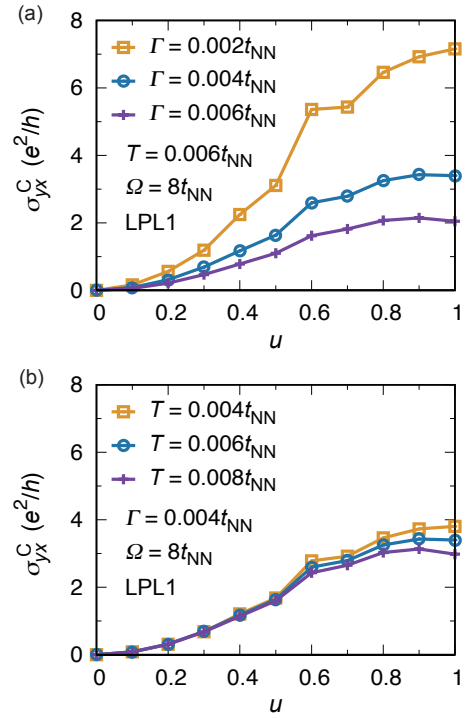


Fig. 3. (Color online) (a), (b) The dependences of σ_{yx}^C on the damping induced by the system-bath coupling, Γ , and the temperature of the bath, T , for graphene driven by LPL1.

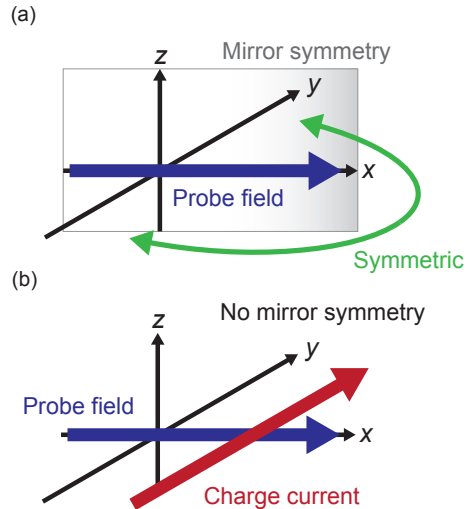


Fig. 4. (Color online) (a), (b) Situations with and without the mirror symmetry (or its combining symmetry with a uniform time translation) under the probe field applied along the x axis.

mirror symmetries and their combining symmetries in the off-diagonal charge conductivity.

5. Discussion

The importance of the mirror symmetry breaking is a general concept. Let us consider a situation where the probe field is applied along the x axis of a material. If the mirror symmetry about the xz plane (or its combining symmetry with a uniform time translation) exists, any currents along the y axis are prohibited [Fig. 4(a)]. Meanwhile, if it is broken, the charge current along the y

axis can be induced [Fig. 4(b)]. This current is finite (i.e., $\sigma_{yx}^C \neq 0$) if the mirror symmetry about the yz plane (or its combining symmetry), as well as that about the xz plane, is broken. Therefore, the mirror symmetry breaking by light plays the key role in the light-induced off-diagonal charge transport. Although mirror symmetry breaking about the xy plane is important in several systems with the Rashba spin-orbit coupling,^{38,39} it is not essential for obtaining σ_{yx}^C and σ_{xy}^C ; such off-site spin-orbit coupling is absent in our system. Note that the importance of the mirror symmetry breaking can be seen from Eq. (8) and the expression using the Berry curvature because both contain the momentum summation of the product of the x and y components of the group velocity, which can be finite without the mirror symmetries about the xz and yz planes and their combining symmetries.

Our results can be tested experimentally. In our system, the nonequilibrium steady state can be achieved due to Γ at times larger than $\tau = \frac{\hbar}{2\Gamma} = O(10\text{fs})$. Then, the off-diagonal charge conductivity in graphene driven by LPL1 could be observed experimentally in pump-probe measurements. Note that $u = \frac{eE_0 a_{\text{NN}}}{\Omega} = 0.1$ at $\Omega = 8t_{\text{NN}} \approx 24 \text{ eV}$ corresponds to $E_0 \approx 171 \text{ MV cm}^{-1}$. In this estimate, we have used $a_{\text{NN}} \approx 0.14 \text{ nm}$.⁴⁰ We have also set $t_{\text{NN}} \approx 3 \text{ eV}$ because, according to the first-principles calculations without $\mathbf{A}(t)$,⁴¹ the energy difference between the two bands in our model at $\mathbf{k} = \mathbf{0}$ corresponds to about 19 eV, i.e., $6t_{\text{NN}} \approx 19 \text{ eV}$. Because of $t_{\text{NN}} \approx 3 \text{ eV}$, $k_{\text{B}}T = 0.006t_{\text{NN}} (\approx 0.018 \text{ eV})$ corresponds to about 209K, where $k_{\text{B}} \approx 8.6 \times 10^{-5} \text{ eV K}^{-1}$ is used. Since σ_{yx}^C and σ_{xy}^C become finite at nonzero u 's [Figs. 2(c) and 2(d)], the off-diagonal charge transport induced by LPL1 is testable.

6. Conclusion

We have studied the polarization dependence of the light-induced mirror symmetry breaking and its effects on charge transport in periodically driven graphene. We showed that the mirror symmetries about the xz and yz planes and their combining symmetries are broken by CPL and by the LPL whose A_x and A_y are both nonzero. This mirror symmetry breaking leads to the light-induced AHE in the absence of the time-reversal symmetry. This indicates that the origin of the light-induced AHE is a combination of the time-reversal symmetry breaking and the mirror symmetry breaking. In the presence of time-reversal symmetry, the mirror symmetry breaking results in the off-diagonal symmetric charge conductivity. This conductivity could be used to detect the mirror symmetry breaking with the time-reversal symmetry. Our results highlight the overlooked role of the light-induced mirror symmetry breaking in the light-induced AHE and reveal the emergence of the off-diagonal symmetric charge transport induced by LPL.

This work was supported by JST CREST Grant No. JPMJCR1901, JSPS KAKENHI Grant No. JP22K03532, and MEXT Q-LEAP Grant No. JP-MXS0118067426.

Appendix A: Light-induced mirror symmetry breaking for the Floquet Hamiltonian

We analyze the polarization dependence of the light-induced mirror symmetry breaking for the Floquet Hamiltonian. As we will show below, this polarization dependence is the same as that for the time-dependent Hamiltonian, which has been shown in the main text. (Note that the Floquet Hamiltonian is distinct from that obtained in a high-frequency expansion.) The momentum dependence of the Floquet Hamiltonian is characterized by

$$\begin{aligned} [\epsilon_{AB}(\mathbf{k})]_{mn} &= \int_0^{T_p} \frac{dt}{T_p} e^{i(m-n)\Omega t} \epsilon_{AB}(\mathbf{k}, t) \\ &= [t_{AB}^Z]_{mn} e^{-ik_y} + [t_{AB}^X]_{mn} e^{i\frac{\sqrt{3}}{2}k_x} e^{i\frac{k_y}{2}} \\ &\quad + [t_{AB}^Y]_{mn} e^{-i\frac{\sqrt{3}}{2}k_x} e^{i\frac{k_y}{2}}, \end{aligned} \quad (\text{A.1})$$

$$\begin{aligned} [\epsilon_{BA}(\mathbf{k})]_{mn} &= \int_0^{T_p} \frac{dt}{T_p} e^{i(m-n)\Omega t} \epsilon_{BA}(\mathbf{k}, t) \\ &= [t_{BA}^Z]_{mn} e^{ik_y} + [t_{BA}^X]_{mn} e^{-i\frac{\sqrt{3}}{2}k_x} e^{-i\frac{k_y}{2}} \\ &\quad + [t_{BA}^Y]_{mn} e^{i\frac{\sqrt{3}}{2}k_x} e^{-i\frac{k_y}{2}}, \end{aligned} \quad (\text{A.2})$$

where

$$[t_{ab}^Z]_{mn} = \int_0^{T_p} \frac{dt}{T_p} e^{i(m-n)\Omega t} t_{ab}^Z(t), \quad (\text{A.3})$$

$$[t_{ab}^X]_{mn} = \int_0^{T_p} \frac{dt}{T_p} e^{i(m-n)\Omega t} t_{ab}^X(t), \quad (\text{A.4})$$

$$[t_{ab}^Y]_{mn} = \int_0^{T_p} \frac{dt}{T_p} e^{i(m-n)\Omega t} t_{ab}^Y(t). \quad (\text{A.5})$$

Note that $\epsilon_{AB}(\mathbf{k}, t)$ and $\epsilon_{BA}(\mathbf{k}, t)$ have been given by Eqs. (3) and (4), respectively. (We neglect the energy shifts due to the light frequency in the Floquet Hamiltonian because such momentum-independent terms do not affect mirror symmetries.) Note that we have considered $[\epsilon_{AB}(\mathbf{k})]_{mn}$ and $[\epsilon_{BA}(\mathbf{k})]_{mn}$ because they give the finite components of $H_{m,n}$, which is part of the matrix used to obtain the quasienergy in the Floquet state.¹¹ As we have explained in the main text, the mirror symmetry about the xz plane is preserved if the hopping integrals as a function of time satisfy Eq. (5). Therefore, for the Floquet Hamiltonian, this mirror symmetry is preserved if

$$[t_{AB}^Z]_{mn} = [t_{BA}^Z]_{mn}, [t_{AB}^Y]_{mn} = [t_{BA}^X]_{mn}, [t_{AB}^X]_{mn} = [t_{BA}^Y]_{mn}. \quad (\text{A.6})$$

In the case of the system driven by LPL described by Eq. (6), the hopping integrals are given by

$$[t_{AB}^Z]_{mn} = t_{\text{NN}} i^{n-m} \mathcal{J}_{m-n}(\alpha_y u), \quad (\text{A.7})$$

$$[t_{AB}^X]_{mn} = t_{\text{NN}} i^{n-m} \mathcal{J}_{n-m} \left(\frac{\sqrt{3}\alpha_x + \alpha_y}{2} u \right), \quad (\text{A.8})$$

$$[t_{AB}^Y]_{mn} = t_{\text{NN}} i^{n-m} \mathcal{J}_{m-n} \left(\frac{\sqrt{3}\alpha_x - \alpha_y}{2} u \right), \quad (\text{A.9})$$

$$[t_{BA}^Z]_{mn} = t_{\text{NN}} i^{n-m} \mathcal{J}_{n-m}(\alpha_y u), \quad (\text{A.10})$$

$$[t_{BA}^X]_{mn} = t_{\text{NN}} i^{n-m} \mathcal{J}_{m-n} \left(\frac{\sqrt{3}\alpha_x + \alpha_y}{2} u \right), \quad (\text{A}\cdot 11)$$

$$[t_{BA}^Y]_{mn} = t_{\text{NN}} i^{n-m} \mathcal{J}_{n-m} \left(\frac{\sqrt{3}\alpha_x - \alpha_y}{2} u \right), \quad (\text{A}\cdot 12)$$

where $\mathcal{J}_l(x)$ is the Bessel function of the first kind with the order l . Therefore, the mirror symmetry about the xz plane is preserved for the LPL with $\alpha_x \neq 0$, $\alpha_y = 0$, whereas it is broken by the LPL with $\alpha_x = 0$, $\alpha_y \neq 0$ or $\alpha_x \neq 0$, $\alpha_y \neq 0$. Similarly, we can show that this mirror symmetry is broken by CPL described by Eq. (7). These results are the same as the polarization dependence shown in the main text.

Appendix B: C_3 rotational symmetry and mirror symmetries without or with a uniform time translation

We discuss the C_3 rotational symmetry, the mirror symmetries, and the combining symmetries with a uniform time translation. First, we show that the C_3 rotational symmetry is broken with CPL or LPL, that the combining symmetry, the symmetry of a combination of the C_3 rotation and a uniform time translation, is preserved with CPL if $T_t : t \rightarrow t + \frac{2\pi}{3\Omega}$, and that the combining symmetry is broken with LPL. Next, we review the mirror symmetry about the xz or yz plane with CPL or LPL, which has been discussed in Sect. III. Then, we show that, as well as the mirror symmetries, the combining symmetries, the symmetries of combinations of the mirror operations about the xz and yz planes and a uniform time translation, are broken with CPL or LPL1. We also show that the symmetry of a combination of the mirror operation about the yz or xz plane and the uniform time translation $T_t : t \rightarrow t - \frac{\pi}{\Omega}$ is preserved with LPL2 or LPL3, respectively. As shown in Sect. III, the mirror symmetry about the yz or xz plane is broken with LPL2 or LPL3, respectively. Note that for LPL1 $\alpha_x \neq 0$ and $\alpha_y \neq 0$ in Eq. (6), for LPL2 $\alpha_x \neq 0$ and $\alpha_y = 0$, and for LPL3 $\alpha_x = 0$ and $\alpha_y \neq 0$.

We begin with the properties about the C_3 rotational symmetry for graphene driven by CPL. This periodically driven system has the C_3 rotational symmetry if the $H_s(t)$ remains unchanged after a counterclockwise rotation of 120 degrees around the z axis. This condition can be expressed as the following equation:

$$C_3^{-1} H_s(t) C_3 = H_s(t). \quad (\text{B}\cdot 1)$$

In the case of graphene, this equation can be rewritten as follows:

$$C_3^{-1} t_{AB}^Z(t) C_3 = t_{AB}^Z(t), \quad (\text{B}\cdot 2)$$

$$C_3^{-1} t_{AB}^X(t) C_3 = t_{AB}^X(t), \quad (\text{B}\cdot 3)$$

$$C_3^{-1} t_{AB}^Y(t) C_3 = t_{AB}^Y(t), \quad (\text{B}\cdot 4)$$

where $t_{AB}^Z(t) = t_{\text{NN}} e^{-ie\mathbf{A}(t)\cdot\mathbf{R}_0}$, $t_{AB}^X(t) = t_{\text{NN}} e^{-ie\mathbf{A}(t)\cdot\mathbf{R}_1}$, and $t_{AB}^Y(t) = t_{\text{NN}} e^{-ie\mathbf{A}(t)\cdot\mathbf{R}_2}$. Since the C_3 rotation transforms the Z , X , and Y bonds on the honeycomb lattice into the X , Y , and Z bonds, respectively [see Fig. 1(a) or 1(b)], the left-hand sides of Eqs. (B.2)–(B.4) become

$$C_3^{-1} t_{AB}^Z(t) C_3 = t_{AB}^X(t), \quad (\text{B}\cdot 5)$$

$$C_3^{-1} t_{AB}^X(t) C_3 = t_{AB}^Y(t), \quad (\text{B}\cdot 6)$$

$$C_3^{-1} t_{AB}^Y(t) C_3 = t_{AB}^Z(t). \quad (\text{B}\cdot 7)$$

Therefore, if the hopping integrals satisfy

$$C_3^{-1} t_{AB}^Z(t) C_3 = t_{AB}^X(t) = t_{AB}^Z(t), \quad (\text{B}\cdot 8)$$

$$C_3^{-1} t_{AB}^X(t) C_3 = t_{AB}^Y(t) = t_{AB}^X(t), \quad (\text{B}\cdot 9)$$

$$C_3^{-1} t_{AB}^Y(t) C_3 = t_{AB}^Z(t) = t_{AB}^Y(t), \quad (\text{B}\cdot 10)$$

the C_3 rotational symmetry is preserved; otherwise, it is broken. Combining Eqs. (B.8)–(B.10) with the equations of the hopping integrals for graphene driven by CPL,

$$t_{AB}^Z(t) = t_{\text{NN}} e^{-iu \sin(\Omega t)}, \quad (\text{B}\cdot 11)$$

$$t_{AB}^X(t) = t_{\text{NN}} e^{-iu \sin(\Omega t - \frac{2\pi}{3})}, \quad (\text{B}\cdot 12)$$

$$t_{AB}^Y(t) = t_{\text{NN}} e^{-iu \sin(\Omega t - \frac{4\pi}{3})}, \quad (\text{B}\cdot 13)$$

we find that these hopping integrals do not satisfy Eqs. (B.8)–(B.10), which means that the C_3 rotational symmetry is broken for graphene driven by CPL. Meanwhile, the periodically driven system has the combining symmetry, the symmetry of a combination of the C_3 rotation and a uniform time translation T_t , if

$$T_t^{-1} C_3^{-1} H_s(t) C_3 T_t = H_s(t), \quad (\text{B}\cdot 14)$$

which is reduced in the case of graphene to

$$T_t^{-1} C_3^{-1} t_{AB}^Z(t) C_3 T_t = t_{AB}^Z(t), \quad (\text{B}\cdot 15)$$

$$T_t^{-1} C_3^{-1} t_{AB}^X(t) C_3 T_t = t_{AB}^X(t), \quad (\text{B}\cdot 16)$$

$$T_t^{-1} C_3^{-1} t_{AB}^Y(t) C_3 T_t = t_{AB}^Y(t). \quad (\text{B}\cdot 17)$$

If we consider the uniform time translation,

$$T_t : t \rightarrow t + \frac{2\pi}{3\Omega}, \quad (\text{B}\cdot 18)$$

the left-hand sides of Eqs. (B.15)–(B.17) are written in graphene driven by CPL as follows:

$$T_t^{-1} C_3^{-1} t_{AB}^Z(t) C_3 T_t = T_t^{-1} t_{AB}^X(t) T_t = t_{AB}^Z(t), \quad (\text{B}\cdot 19)$$

$$T_t^{-1} C_3^{-1} t_{AB}^X(t) C_3 T_t = T_t^{-1} t_{AB}^Y(t) T_t = t_{AB}^X(t), \quad (\text{B}\cdot 20)$$

$$T_t^{-1} C_3^{-1} t_{AB}^Y(t) C_3 T_t = T_t^{-1} t_{AB}^Z(t) T_t = t_{AB}^Y(t), \quad (\text{B}\cdot 21)$$

where we have used Eqs. (B.5)–(B.7) and (B.11)–(B.13). Therefore, the combining symmetry, which may be called a time-screw symmetry, is preserved for graphene driven by CPL. Because of this property, the time-averaged off-diagonal charge conductivities in the nonequilibrium steady state with CPL satisfy $\sigma_{xy}^C = -\sigma_{yx}^C$ even without using the Onsager reciprocal relation.

In a similar way, we can show for graphene driven by LPL that the C_3 rotational symmetry and its combining symmetry are both broken. This result holds for arbitrary α_x and α_y of Eq. (6). Because of the breaking of these symmetries, there is no need to satisfy $\sigma_{xy}^C = -\sigma_{yx}^C$ in the case of LPL. Namely, $\sigma_{xy}^C = \sigma_{yx}^C$ with LPL1 is symmetrically reasonable. Note that for graphene driven by LPL the hopping integrals are given by

$$t_{AB}^Z(t) = t_{\text{NN}} e^{-iu\alpha_y \cos(\Omega t)}, \quad (\text{B}\cdot 22)$$

$$t_{AB}^X(t) = t_{\text{NN}} e^{iu\frac{\sqrt{3}}{2}\alpha_x \cos(\Omega t)} e^{iu\frac{\alpha_y}{2} \cos(\Omega t)}, \quad (\text{B}\cdot 23)$$

$$t_{AB}^Y(t) = t_{\text{NN}} e^{-iu\frac{\sqrt{3}}{2}\alpha_x \cos(\Omega t)} e^{iu\frac{\alpha_y}{2} \cos(\Omega t)}. \quad (\text{B}\cdot 24)$$

We turn to the properties of the mirror symmetry about the xz or yz plane. The periodically driven system is symmetric with respect to the xz mirror plane [Fig. 1(a)] if

$$\sigma_m^{-1} H_s(t) \sigma_m = H_s(t), \quad (\text{B}\cdot 25)$$

which is written in the case of graphene as

$$\sigma_m^{-1} t_{AB}^Z(t) \sigma_m = t_{AB}^Z(t), \quad (\text{B}\cdot 26)$$

$$\sigma_m^{-1} t_{AB}^X(t) \sigma_m = t_{AB}^X(t), \quad (\text{B}\cdot 27)$$

$$\sigma_m^{-1} t_{AB}^Y(t) \sigma_m = t_{AB}^Y(t). \quad (\text{B}\cdot 28)$$

As we can see from Fig. 1(a), the left-hand sides of these equations become

$$\sigma_m^{-1} t_{AB}^Z(t) \sigma_m = t_{BA}^Z(t), \quad (\text{B}\cdot 29)$$

$$\sigma_m^{-1} t_{AB}^X(t) \sigma_m = t_{BA}^Y(t), \quad (\text{B}\cdot 30)$$

$$\sigma_m^{-1} t_{AB}^Y(t) \sigma_m = t_{BA}^X(t). \quad (\text{B}\cdot 31)$$

A combination of Eqs. (B·26)–(B·28) and Eqs. (B·29)–(B·31) gives Eq. (5). Therefore, as we have shown in Sect. III, the mirror symmetry about the xz plane is broken for graphene driven by CPL and LPL with $\alpha_y \neq 0$, whereas it is preserved for graphene driven by LPL with $\alpha_y = 0$ (see Table I). For the mirror symmetry about the yz plane, Eqs. (B·25) and (B·26)–(B·28) are replaced by

$$(\sigma'_m)^{-1} H_s(t) \sigma'_m = H_s(t), \quad (\text{B}\cdot 32)$$

and

$$(\sigma'_m)^{-1} t_{AB}^Z(t) \sigma'_m = t_{AB}^Z(t), \quad (\text{B}\cdot 33)$$

$$(\sigma'_m)^{-1} t_{AB}^X(t) \sigma'_m = t_{AB}^X(t), \quad (\text{B}\cdot 34)$$

$$(\sigma'_m)^{-1} t_{AB}^Y(t) \sigma'_m = t_{AB}^Y(t). \quad (\text{B}\cdot 35)$$

Moreover, as we can see from Fig. 1(b), the left-hand sides of Eqs. (B·33)–(B·35) are expressed as

$$(\sigma'_m)^{-1} t_{AB}^Z(t) \sigma'_m = t_{AB}^Z(t), \quad (\text{B}\cdot 36)$$

$$(\sigma'_m)^{-1} t_{AB}^X(t) \sigma'_m = t_{AB}^Y(t), \quad (\text{B}\cdot 37)$$

$$(\sigma'_m)^{-1} t_{AB}^Y(t) \sigma'_m = t_{AB}^X(t). \quad (\text{B}\cdot 38)$$

Therefore, as we have remarked in Sect. III, the mirror symmetry about the yz plane is broken for graphene driven by CPL or LPL with $\alpha_x \neq 0$, whereas it is preserved for graphene driven by LPL with $\alpha_x = 0$ (see Table I). Then, for the combining symmetry for the xz mirror plane, Eqs. (B·25) and (B·32) are replaced by

$$T_t^{-1} \sigma_m^{-1} H_s(t) \sigma_m T_t = H_s(t), \quad (\text{B}\cdot 39)$$

and

$$T_t^{-1} (\sigma'_m)^{-1} H_s(t) \sigma'_m T_t = H_s(t), \quad (\text{B}\cdot 40)$$

respectively. In the case of graphene, the former is decomposed into

$$T_t^{-1} \sigma_m^{-1} t_{AB}^Z(t) \sigma_m T_t = T_t^{-1} t_{BA}^Z(t) T_t = t_{AB}^Z(t), \quad (\text{B}\cdot 41)$$

$$T_t^{-1} \sigma_m^{-1} t_{AB}^X(t) \sigma_m T_t = T_t^{-1} t_{BA}^Y(t) T_t = t_{AB}^X(t), \quad (\text{B}\cdot 42)$$

$$T_t^{-1} \sigma_m^{-1} t_{AB}^Y(t) \sigma_m T_t = T_t^{-1} t_{BA}^X(t) T_t = t_{AB}^Y(t), \quad (\text{B}\cdot 43)$$

and the latter is decomposed into

$$T_t^{-1} (\sigma'_m)^{-1} t_{AB}^Z(t) \sigma'_m T_t = T_t^{-1} t_{AB}^Z(t) T_t = t_{AB}^Z(t), \quad (\text{B}\cdot 44)$$

$$T_t^{-1} (\sigma'_m)^{-1} t_{AB}^X(t) \sigma'_m T_t = T_t^{-1} t_{AB}^Y(t) T_t = t_{AB}^X(t), \quad (\text{B}\cdot 45)$$

$$T_t^{-1} (\sigma'_m)^{-1} t_{AB}^Y(t) \sigma'_m T_t = T_t^{-1} t_{AB}^X(t) T_t = t_{AB}^Y(t). \quad (\text{B}\cdot 46)$$

In deriving the first and the last three equations, we have used Eqs. (B·29)–(B·31) and Eqs. (B·36)–(B·38), respectively. Using Eqs. (B·11)–(B·13) or (B·22)–(B·24), we can show that the combining symmetries for the xz and yz mirror planes are broken for graphene driven by CPL or LPL1. This is because in the case of graphene driven by CPL or LPL1, there is no uniform time translation which makes the system after the mirror operation the same as that before it. For example, in the case of the mirror symmetry about the yz plane with CPL, if we choose T_t in Eqs. (B·44)–(B·46) as Eq. (B·18), we get

$$\begin{aligned} T_t^{-1} (\sigma'_m)^{-1} t_{AB}^Z(t) \sigma'_m T_t &= T_t^{-1} t_{AB}^Z(t) T_t \\ &= t_{\text{NN}} e^{-iu \sin(\Omega t + \frac{2\pi}{3})} = t_{AB}^Y(t) \neq t_{AB}^Z(t), \end{aligned} \quad (\text{B}\cdot 47)$$

$$\begin{aligned} T_t^{-1} (\sigma'_m)^{-1} t_{AB}^X(t) \sigma'_m T_t &= T_t^{-1} t_{AB}^Y(t) T_t \\ &= t_{\text{NN}} e^{-iu \sin(\Omega t - \frac{2\pi}{3})} = t_{AB}^X(t), \end{aligned} \quad (\text{B}\cdot 48)$$

$$\begin{aligned} T_t^{-1} (\sigma'_m)^{-1} t_{AB}^Y(t) \sigma'_m T_t &= T_t^{-1} t_{AB}^X(t) T_t \\ &= t_{\text{NN}} e^{-iu \sin(\Omega t)} = t_{AB}^Z(t) \neq t_{AB}^Y(t). \end{aligned} \quad (\text{B}\cdot 49)$$

There is no uniform time translation that the three conditions for the hopping integrals are satisfied simultaneously. In contrast, the combining symmetry for the yz or xz mirror plane is preserved in graphene driven by LPL2 or LPL3, respectively. As we have shown in Sect. III, the mirror symmetry about the xz plane is preserved for graphene driven by LPL2, whereas it is broken for graphene driven by LPL3. Meanwhile, the hopping integrals for graphene driven by LPL3 satisfy Eqs. (B·41)–(B·43) if the T_t is chosen as

$$T_t : t \rightarrow t - \frac{\pi}{\Omega}. \quad (\text{B}\cdot 50)$$

By using the same T_t , we can show that the hopping integrals for graphene driven by LPL2 satisfy Eqs. (B·44)–(B·46). Therefore, the symmetry of a combination of the mirror operation about the yz or xz plane and the uniform time translation of Eq. (B·50), which may be called a time-glide symmetry, is preserved for graphene driven by LPL2 or LPL3, respectively.

Appendix C: Derivation of Eq. (8)

We derive Eq. (8). Since this derivation has been explained, for example, in Ref.,¹²⁾ we explain the main points below. Treating $\mathbf{A}_{\text{prob}}(t)$ in the linear-response

theory, we express a charge conductivity as

$$\sigma_{\mu\nu}^C(t, t') = \frac{1}{i\omega} \frac{\delta \langle j_C^\mu(t) \rangle}{\delta A_{\text{prob}}^\nu(t')}, \quad (\text{C.1})$$

where $\langle j_C^\mu(t) \rangle$ is the expectation value of the operator of the charge current density $j_C^\mu(t) = J_C^\mu(t)/V$, $J_C^\mu(t)$ is the charge current operator,

$$J_C^\mu(t) = (-e) \sum_{\mathbf{k}} \sum_{a,b} \sum_{\sigma=\uparrow,\downarrow} v_{ab}^\mu(\mathbf{k}, t) c_{\mathbf{k}a\sigma}^\dagger(t) c_{\mathbf{k}b\sigma}(t), \quad (\text{C.2})$$

and $v_{ab}^\mu(\mathbf{k}, t) = \frac{\partial \epsilon_{ab}(\mathbf{k}, t)}{\partial k_\mu}$. By substituting Eq. (C.2) into Eq. (C.1) and doing some calculations,¹²⁾ we get

$$\sigma_{\mu\nu}^C(t, t') = \sigma_{\mu\nu}^{C(1)}(t, t') + \sigma_{\mu\nu}^{C(2)}(t, t'), \quad (\text{C.3})$$

where

$$\sigma_{\mu\nu}^{C(1)}(t, t') = \frac{e}{\omega V} \sum_{\mathbf{k}} \sum_{a,b} \sum_{\sigma=\uparrow,\downarrow} \frac{\delta v_{ab}^\mu(\mathbf{k}, t)}{\delta A_{\text{prob}}^\nu(t')} G_{b\sigma a\sigma}^<(\mathbf{k}; t, t'), \quad (\text{C.4})$$

$$\begin{aligned} \sigma_{\mu\nu}^{C(2)}(t, t') &= \frac{(-e)^2}{\omega V} \sum_{\mathbf{k}} \sum_{a,b,c,d} \sum_{\sigma,\sigma'=\uparrow,\downarrow} v_{ab}^\mu(\mathbf{k}, t) v_{cd}^\nu(\mathbf{k}, t') \\ &\times \left[G_{b\sigma c\sigma'}^R(\mathbf{k}; t, t') G_{d\sigma' a\sigma}^<(\mathbf{k}; t', t) \right. \\ &\left. + G_{b\sigma c\sigma'}^<(\mathbf{k}; t, t') G_{d\sigma' a\sigma}^A(\mathbf{k}; t', t) \right], \quad (\text{C.5}) \end{aligned}$$

and the lesser, retarded, and advanced Green's functions are defined as follows:

$$G_{b\sigma' a\sigma}^<(\mathbf{k}; t, t') = i \langle c_{\mathbf{k}a\sigma}^\dagger(t') c_{\mathbf{k}b\sigma'}(t) \rangle, \quad (\text{C.6})$$

$$G_{a\sigma b\sigma'}^R(\mathbf{k}; t, t') = -i\theta(t - t') \langle \{ c_{\mathbf{k}a\sigma}(t), c_{\mathbf{k}b\sigma'}^\dagger(t') \} \rangle, \quad (\text{C.7})$$

$$G_{a\sigma b\sigma'}^A(\mathbf{k}; t, t') = i\theta(t' - t) \langle \{ c_{\mathbf{k}a\sigma}(t), c_{\mathbf{k}b\sigma'}^\dagger(t') \} \rangle. \quad (\text{C.8})$$

Since we consider charge transport in the nonequilibrium steady state, we introduce the time-averaged charge conductivity,

$$\sigma_{\mu\nu}^C = \lim_{\omega \rightarrow 0} \text{Re} \int_0^{T_p} \frac{dt_{\text{av}}}{T_p} \int_{-\infty}^{\infty} dt_{\text{rel}} e^{i\omega t_{\text{rel}}} \sigma_{\mu\nu}^C(t, t'), \quad (\text{C.9})$$

where $t_{\text{rel}} = t - t'$ and $t_{\text{av}} = (t + t')/2$. By combining Eq. (C.9) with Eqs. (C.3)–(C.5) and performing some calculations,¹²⁾ we obtain

$$\begin{aligned} \sigma_{\mu\nu}^C &= \frac{(-e)^2}{V} \sum_{\mathbf{k}} \sum_{a,b,c,d} \sum_{\sigma,\sigma'=\uparrow,\downarrow} \int_{-\Omega/2}^{\Omega/2} \frac{d\omega'}{2\pi} \sum_{m,l,n,q=-\infty}^{\infty} \\ &\times \left\{ [v_{ab}^\mu(\mathbf{k})]_{ml} \frac{\partial [G_{b\sigma c\sigma'}^R(\mathbf{k}, \omega')]_{ln}}{\partial \omega'} [v_{cd}^\nu(\mathbf{k})]_{nq} [G_{d\sigma' a\sigma}^<(\mathbf{k}, \omega')]_{qm} \right. \\ &\left. - [v_{ab}^\mu(\mathbf{k})]_{ml} [G_{b\sigma c\sigma'}^<(\mathbf{k}, \omega')]_{ln} [v_{cd}^\nu(\mathbf{k})]_{nq} \frac{\partial [G_{d\sigma' a\sigma}^A(\mathbf{k}, \omega')]_{qm}}{\partial \omega'} \right\}, \quad (\text{C.10}) \end{aligned}$$

where the group velocity and Green's functions in the Floquet representation are defined as

$$[v_{ab}^\mu(\mathbf{k})]_{mn} = \int_0^{T_p} \frac{dt}{T_p} e^{i(m-n)\Omega t} v_{ab}^\mu(\mathbf{k}, t), \quad (\text{C.11})$$

$$[G_{a\sigma b\sigma'}^r(\mathbf{k}, \omega')]_{mn} = \int_{-\infty}^{\infty} dt_{\text{rel}} e^{i(\omega' + \frac{m+n}{2}\Omega)t_{\text{rel}}} \int_0^{T_p} \frac{dt_{\text{av}}}{T_p}$$

$$\times e^{i(m-n)\Omega t_{\text{av}}} G_{a\sigma b\sigma'}^r(\mathbf{k}; t, t'). \quad (\text{C.12})$$

Equation (C.10) is equivalent to Eq. (8).

Appendix D: Dyson's equation for the Green's functions

The Green's functions appearing in Eq. (8) are determined from Dyson's equation in a matrix form,¹²⁾

$$G = G_0 + G_0 \Sigma G, \quad (\text{D.1})$$

where

$$G = \begin{pmatrix} G^R & G^K \\ 0 & G^A \end{pmatrix}, \quad G_0 = \begin{pmatrix} G_0^R & G_0^K \\ 0 & G_0^A \end{pmatrix}, \quad \Sigma = \begin{pmatrix} \Sigma^R & \Sigma^K \\ 0 & \Sigma^A \end{pmatrix}. \quad (\text{D.2})$$

Here G^R , G^A , and G^K are the retarded, advanced, and Keldysh Green's functions with H_{sb} , G_0^R , G_0^A , and G_0^K are those without H_{sb} , and Σ^R , Σ^A , and Σ^K are the retarded, advanced, and Keldysh self-energies due to the second-order perturbation of H_{sb} ; the matrix G^R is, for instance, given by $G^R = ([G_{a\sigma b\sigma'}^R(\mathbf{k}, \omega)]_{mn})$, where $a, b = A, B, \sigma, \sigma' = \uparrow, \downarrow$, and $m, n = -\infty, \dots, 0, 1, \dots, \infty$. The retarded, advanced, and Keldysh components are related to the lesser component via the relation, such as

$$G^< = \frac{1}{2}(G^K - G^R + G^A). \quad (\text{D.3})$$

In the second-order perturbation theory, in which H_{sb} is treated as perturbation, Σ^R , Σ^A , and Σ^K are given by¹²⁾

$$[\Sigma_{a\sigma b\sigma'}^R(\mathbf{k}, \omega)]_{mn} = -i\delta_{m,n} \delta_{a,b} \delta_{\sigma,\sigma'} \Gamma, \quad (\text{D.4})$$

$$[\Sigma_{a\sigma b\sigma'}^A(\mathbf{k}, \omega)]_{mn} = +i\delta_{m,n} \delta_{a,b} \delta_{\sigma,\sigma'} \Gamma, \quad (\text{D.5})$$

$$[\Sigma_{a\sigma b\sigma'}^K(\mathbf{k}, \omega)]_{mn} = -2i\Gamma \delta_{m,n} \delta_{a,b} \delta_{\sigma,\sigma'} \tanh \frac{\omega + m\Omega}{2T}, \quad (\text{D.6})$$

where Γ is the damping. Then, the matrices G^R , G^A , and G^K can be determined from the following relations:¹²⁾

$$(G^R)^{-1} = (G^{-1})^R, \quad (\text{D.7})$$

$$(G^A)^{-1} = (G^{-1})^A, \quad (\text{D.8})$$

$$G^K = -G^R (G^{-1})^K G^A, \quad (\text{D.9})$$

where

$$G^{-1} = \begin{pmatrix} (G^{-1})^R & (G^{-1})^K \\ 0 & (G^{-1})^A \end{pmatrix}. \quad (\text{D.10})$$

Therefore, we obtain the retarded and advanced Green's functions with H_{sb} using Eqs. (D.7) and (D.8) with the equations,

$$\begin{aligned} [(G^{-1})_{a\sigma b\sigma'}^R(\mathbf{k}, \omega)]_{mn} &= (\omega + m\Omega + i\Gamma) \delta_{m,n} \delta_{a,b} \delta_{\sigma,\sigma'} \\ &- [\epsilon_{ab}(\mathbf{k})]_{mn} \delta_{\sigma,\sigma'}, \quad (\text{D.11}) \end{aligned}$$

$$\begin{aligned} [(G^{-1})_{a\sigma b\sigma'}^A(\mathbf{k}, \omega)]_{mn} &= (\omega + m\Omega - i\Gamma) \delta_{m,n} \delta_{a,b} \delta_{\sigma,\sigma'} \\ &- [\epsilon_{ab}(\mathbf{k})]_{mn} \delta_{\sigma,\sigma'}, \quad (\text{D.12}) \end{aligned}$$

where

$$[\epsilon_{ab}(\mathbf{k})]_{mn} = \int_0^{T_p} \frac{dt}{T_p} e^{i(m-n)\Omega t} \epsilon_{ab}(\mathbf{k}, t). \quad (\text{D.13})$$

We also get the Keldysh Green's function with H_{sb} using these Green's functions, Eq. (D.9), and

$$[(G^{-1})_{\alpha\sigma b\sigma'}^{\text{K}}(\mathbf{k}, \omega)]_{mn} = 2i\Gamma\delta_{m,n}\delta_{a,b}\delta_{\sigma,\sigma'} \tanh \frac{\omega + m\Omega}{2T}. \quad (\text{D.14})$$

Then, using these three Green's functions and Eq. (D.3), we obtain the lesser Green's function with H_{sb} .

Appendix E: Details of the numerical calculations

We numerically calculate $\sigma_{\mu\nu}^{\text{C}}$ of Eq. (8) in the following procedure. To calculate the momentum summation, we set $\mathbf{k} = \frac{m_1}{N_1}\mathbf{b}_1 + \frac{m_2}{N_2}\mathbf{b}_2$ and $N_1 = N_2 = 360$, where $0 \leq m_1 < N_1$, $0 \leq m_2 < N_2$, $\mathbf{b}_1 = t(\frac{2\pi}{\sqrt{3}} \frac{2\pi}{3})$, $\mathbf{b}_2 = t(\frac{2\pi}{\sqrt{3}} - \frac{2\pi}{3})$, and $N_1N_2 = \frac{N}{2}$. We calculated the frequency integral using $\int_{-\Omega/2}^{\Omega/2} d\omega' F(\omega') \approx \sum_{s=0}^{W-1} \Delta\omega' F(\omega'_s)$, where $\omega'_s = -\Omega/2 + s\Delta\omega'$, $\omega'_W = \Omega/2$, and $\Delta\omega' = 0.001t_{\text{NN}}$. Then, to calculate the frequency derivatives of the Green's functions, we used $\frac{\partial F(\omega')}{\partial \omega'} \approx \frac{F(\omega' + \Delta\omega') - F(\omega' - \Delta\omega')}{2\Delta\omega'}$. We took the trace over the Floquet states [i.e., $\text{tr}(ABCD) = \sum_{m,l,n,q=-\infty}^{\infty} A_{ml}B_{ln}C_{nq}D_{qm}$], replaced the summation over the Floquet indices, $\sum_{m,l,n,q=-\infty}^{\infty}$, by $\sum_{m,l,n,q=-n_{\text{max}}}^{n_{\text{max}}}$, and set $n_{\text{max}} = 2$.

Appendix F: Additional numerical results

We show additional numerical results. Figure F.1(a) compares the u dependences of σ_{yx}^{C} in graphene driven by the LPL for $\alpha_x = \alpha_y = 1$, which has been considered as the case of LPL1 in the main text, and by the LPL for $\alpha_x = -\alpha_y = 1$. (Note that in both cases the mirror symmetries about the xz and yz planes and their combining symmetries are both broken, which means that the latter LPL also belongs to LPL1.) The σ_{yx}^{C} 's in these two cases are the same in magnitude and opposite in sign. In addition, $\sigma_{yx}^{\text{C}} = \sigma_{xy}^{\text{C}}$ holds in both cases, as shown in Fig. F.1(b). We should note that the systems driven by the LPL for $\alpha_x = \alpha_y = 1$ and by the LPL for $\alpha_x = -\alpha_y = 1$ are connected by a mirror operation with respect to the xz plane, which interchanges parts of the system above and below the xz mirror plane of Fig. 1(a). This is because this mirror operation replaces $t_{AB}^Z(t)$, $t_{AB}^X(t)$, and $t_{AB}^Y(t)$ by $t_{BA}^Z(t)$, $t_{BA}^X(t)$, and $t_{BA}^Y(t)$, respectively [see Eq. (5)] and $t_{BA}^Z(t)$, $t_{BA}^X(t)$, and $t_{BA}^Y(t)$ in the former case are the same as $t_{AB}^Z(t)$, $t_{AB}^X(t)$, and $t_{AB}^Y(t)$ in the latter case. Note that these hopping integrals with the LPL for $\alpha_x = \alpha_y = 1$ are given by

$$\begin{aligned} t_{AB}^Z(t) &= t_{\text{NN}}e^{-iu \cos \Omega t}, \\ t_{AB}^X(t) &= t_{\text{NN}}e^{iu \frac{\sqrt{3}}{2} \cos \Omega t} e^{iu \frac{1}{2} \cos \Omega t}, \\ t_{AB}^Y(t) &= t_{\text{NN}}e^{-iu \frac{\sqrt{3}}{2} \cos \Omega t} e^{iu \frac{1}{2} \cos \Omega t}, \end{aligned} \quad (\text{F.1})$$

$$\begin{aligned} t_{BA}^Z(t) &= t_{\text{NN}}e^{iu \cos \Omega t}, \\ t_{BA}^X(t) &= t_{\text{NN}}e^{-iu \frac{\sqrt{3}}{2} \cos \Omega t} e^{-iu \frac{1}{2} \cos \Omega t}, \\ t_{BA}^Y(t) &= t_{\text{NN}}e^{iu \frac{\sqrt{3}}{2} \cos \Omega t} e^{-iu \frac{1}{2} \cos \Omega t}, \end{aligned} \quad (\text{F.2})$$

whereas those with the LPL for $\alpha_x = -\alpha_y = 1$ are given by

$$\begin{aligned} t_{AB}^Z(t) &= t_{\text{NN}}e^{iu \cos \Omega t}, \\ t_{AB}^X(t) &= t_{\text{NN}}e^{iu \frac{\sqrt{3}}{2} \cos \Omega t} e^{-iu \frac{1}{2} \cos \Omega t}, \\ t_{AB}^Y(t) &= t_{\text{NN}}e^{-iu \frac{\sqrt{3}}{2} \cos \Omega t} e^{-iu \frac{1}{2} \cos \Omega t}, \end{aligned} \quad (\text{F.3})$$

$$\begin{aligned} t_{BA}^Z(t) &= t_{\text{NN}}e^{-iu \cos \Omega t}, \\ t_{BA}^X(t) &= t_{\text{NN}}e^{-iu \frac{\sqrt{3}}{2} \cos \Omega t} e^{iu \frac{1}{2} \cos \Omega t}, \\ t_{BA}^Y(t) &= t_{\text{NN}}e^{iu \frac{\sqrt{3}}{2} \cos \Omega t} e^{iu \frac{1}{2} \cos \Omega t}. \end{aligned} \quad (\text{F.4})$$

Moreover, Figs. F.1(c) and F.1(d) show that the sign of $\sigma_{yx}^{\text{C}} (= \sigma_{xy}^{\text{C}})$ can be reversed by changing from the LPL for $\alpha_x = \alpha_y = 1$ to that for $-\alpha_x = \alpha_y = 1$. This result can be similarly understood because the system driven by the LPL for $-\alpha_x = \alpha_y = 1$ is a counterpart connected by the mirror operation about the yz plane. Then, $\sigma_{yx}^{\text{C}} (= \sigma_{xy}^{\text{C}})$ driven by the LPL for $\alpha_x = \alpha_y = -1$ becomes the same as that for $\alpha_x = \alpha_y = 1$, as shown in Figs. F.1(e) and F.1(f). This is because the system driven by the LPL for $\alpha_x = \alpha_y = -1$ is connected to that driven by the LPL for $\alpha_x = -\alpha_y = 1$ by the mirror operation about the yz plane (or to that driven by the LPL for $-\alpha_x = \alpha_y = 1$ by the mirror operation about the xz plane). The similar properties hold in more general cases in which α_x and α_y are written as $\alpha_x = \cos \theta$ and $\alpha_y = \sin \theta$, as shown in Figs. F.2(a) and F.2(b). Namely, $\sigma_{yx}^{\text{C}} (= \sigma_{xy}^{\text{C}})$'s driven by the LPL for $\theta = \theta_0$ and $\theta_0 + 180^\circ$ (e.g., $\theta = 30^\circ$ and 210°) are the same in magnitude and sign, whereas those for $\theta = 360^\circ - \theta_0$ and $180^\circ - \theta_0$ (e.g., $\theta = 330^\circ$ and 150°) have the opposite sign to $\theta = \theta_0$ and $\theta_0 + 180^\circ$ and the same magnitude; these properties can be understood in a similar way. Therefore, these results indicate that the sign of the off-diagonal symmetric charge conductivity can be changed by switching LPL1 to a counterpart connected by the mirror operation about the xz or yz plane. Note that the relation between the LPL for $\alpha_x = \alpha_y = 1$ and for $\alpha_x = -\alpha_y = 1$ is similar to that between left- and right-handed circularly polarized light because the systems driven by left- and right-handed circularly polarized light are connected by the mirror operation (and also by a time-reversal operation¹²).

-
- 1) Y. H. Wang, H. Steinberg, P. Jarillo-Herrero, and N. Gedik, *Science* **342**, 453-457 (2013).
 - 2) M. Claassen, H.-C. Jiang, B. Moritz, and T. P. Devereaux, *Nat. Commun.* **8**, 1192 (2017).
 - 3) S. Kitamura, T. Oka, and H. Aoki, *Phys. Rev. B* **96**, 014406 (2017).
 - 4) J. P. van der Ziel, P. S. Pershan, and L. D. Malmstrom, *Phys. Rev. Lett.* **15**, 190 (1965).
 - 5) A. V. Kimel, A. Kirilyuk, P. A. Usachev, R. V. Pisarev, A. M. Balbashov, and Th. Rasing, *Nature* **435**, 655-657 (2005).
 - 6) T. Oka and H. Aoki, *Phys. Rev. B* **79**, 081406(R) (2009).
 - 7) J. W. McIver, B. Schulte, F.-U. Stein, T. Matsuyama, G. Jotzu, G. Meier, and A. Cavalleri, *Nat. Phys.* **16**, 38-41 (2020).
 - 8) E. H. Hall, *Philos. Mag.* **12**, 157 (1881).
 - 9) R. Karplus and J. M. Luttinger, *Phys. Rev.* **95**, 1154 (1954).
 - 10) N. Nagaosa, J. Sinova, S. Onoda, A. H. MacDonald, and N. P.

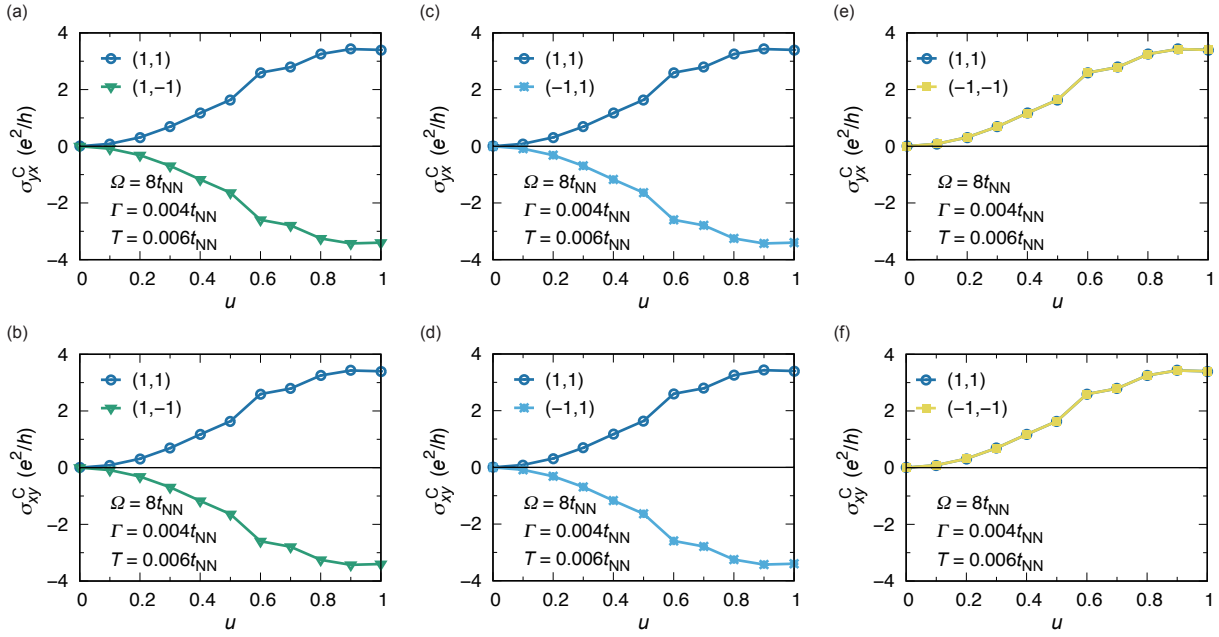


Fig. F.1. (Color online) (a)–(f) The polarization dependences of σ_{yx}^C and σ_{xy}^C as functions of $u = eA_0$ for graphene driven by LPL. The blue, green, light blue, and yellow lines correspond to the cases with the LPL for $\alpha_x = \alpha_y = 1$, for $\alpha_x = -\alpha_y = 1$, for $-\alpha_x = \alpha_y = 1$, and for $\alpha_x = \alpha_y = -1$, respectively.

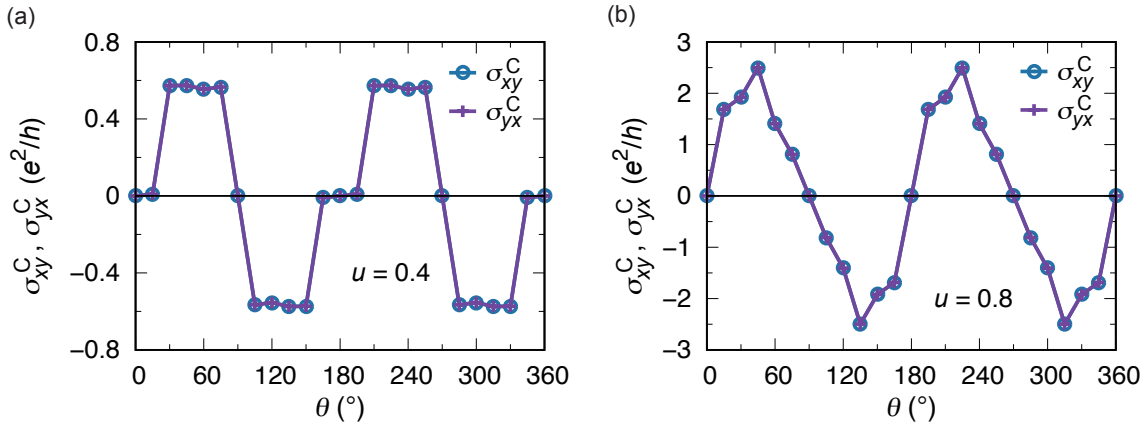


Fig. F.2. (Color online) The θ dependences of σ_{yx}^C and σ_{xy}^C at (a) $u = 0.4$ and (b) $u = 0.8$ in graphene driven by LPL for $\alpha_x = \cos \theta$ and $\alpha_y = \sin \theta$. In these panels, $\Omega = 8t_{NN}$, $\Gamma = 0.004t_{NN}$, and $T = 0.006t_{NN}$.

- Ong, *Rev. Mod. Phys.* **82**, 1539 (2010).
- 11) T. Mikami, S. Kitamura, K. Yasuda, N. Tsuji, T. Oka, and H. Aoki, *Phys. Rev. B* **93**, 144307 (2016).
 - 12) N. Arakawa and K. Yonemitsu, *Comms. Phys.* **6**, 43 (2023).
 - 13) O. Kfir, P. Grychtol, E. Turgut, R. Knut, D. Zusin, D. Popmintchev, T. Popmintchev, H. Nembach, J. M. Shaw, A. Fleischer, H. Kapteyn, M. Murnane, and O. Cohen, *Nat. Photonics* **9**, 99 (2015).
 - 14) T. Nag, R.-J. Slager, T. Higuchi, and T. Oka, *Phys. Rev. B* **100**, 134301 (2019).
 - 15) T. V. Trevisan, P. V. Arribi, O. Heinonen, R.-J. Slager, and P. P. Orth, *Phys. Rev. Lett.* **128**, 066602 (2022).
 - 16) Y. Ikeda, S. Kitamura, and T. Morimoto, *Prog. Theor. Exp. Phys.* **2022**, 04A101 (2022).
 - 17) D. S. L. Abergel, V. Apalkov, J. Berashevich, K. Ziegler, and T. Chakraborty, *Advances in Physics*, **59**, 261-482 (2010).
 - 18) M. Büttiker, *Phys. Rev. B* **32**, 1846(R) (1985).
 - 19) M. Büttiker, *Phys. Rev. B* **33**, 3020 (1986).
 - 20) N. Tsuji, T. Oka, and H. Aoki, *Phys. Rev. Lett.* **103**, 047403 (2009).
 - 21) L. D'Alessio and M. Rigol, *Phys. Rev. X* **4**, 041048 (2014).
 - 22) A. Lazarides, A. Das, and R. Moessner, *Phys. Rev. E* **90**, 012110 (2014).
 - 23) L. Du, Q. Chen, A. D. Barr, A. R. Barr, and G. A. Fiete, *Phys. Rev. B* **98**, 245145 (2018).
 - 24) M. Eckstein and M. Kollar, *Phys. Rev. B* **78**, 205119 (2008).
 - 25) J. H. Shirley, *Phys. Rev.* **138**, B979 (1965).
 - 26) H. Sambe, *Phys. Rev. A* **7**, 2203 (1973).
 - 27) R. Kubo, *J. Phys. Soc. Jpn.* **12**, 570 (1957).
 - 28) A. Kirilyuk, A. V. Kimel, and T. Rasing, *Rev. Mod. Phys.* **82**, 2731 (2010).
 - 29) L. Onsager, *Phys. Rev.* **37**, 405 (1931).
 - 30) L. Onsager, *Phys. Rev.* **38**, 2265 (1931).
 - 31) H. Kontani, T. Tanaka, and K. Yamada, *Phys. Rev. B* **75**, 184416 (2007).
 - 32) T. Tomizawa and H. Kontani, *Phys. Rev. B* **80**, 100401(R) (2009).
 - 33) F. Schindler, A. M. Cook, M. G. Vergniory, Z. Wang, S. S. P. Parkin, B. A. Bernevig, and T. Neupert, *Sci. Adv.* **4**, eaat0346 (2018).
 - 34) A. Eckardt and E. Anisimovas, *New J. Phys.* **17**, 093039 (2015).
 - 35) M. Bukov, L. D'Alessio, and A. Polkovnikov, *Adv. Phys.* **64**, 139 (2015).
 - 36) T. Kitagawa, T. Oka, A. Brataas, L. Fu, and E. Demler, *Phys. Rev. B* **84**, 235108 (2011).
 - 37) F. D. M. Haldane, *Phys. Rev. Lett.* **61**, 2015 (1988).
 - 38) V. M. Edelstein, *Phys. Rev. Lett.* **95**, 156602 (2005).
 - 39) H. Chen, Q. Niu, and A. H. MacDonald, *Phys. Rev. Lett.* **112**, 017205 (2014).
 - 40) G. Yang, L. Li, W. B. Lee, and M. C. Ng, *Sci. Tech. Adv. Mat.* **19**, 613-648 (2018).
 - 41) E. Kogan, V. U. Nazarov, V. M. Silkin, and M. Kaveh, *Phys. Rev. B* **89**, 165430 (2014).